Volume 1 | Number 1 | Jan 2013 | Pages 1–100

PCCP

Physical Chemistry Chemical Physics
www.rsc.org/pccp

ROYAL SOCIETY OF CHEMISTRY

ROYAL SOCIETY OF CHEMISTRY

www.rsc.org/pccp

Physical Chemistry Chemical Physics

ARTICLE

Accurate calculation of the band gap of liquid water by means of GW corrections applied to plane-wave density functional theory molecular dynamics simulations

Changming Fang[1*], Wun-Fan Li[1], Rik S. Koster[1], Jiří Klimeš[2], Alfons van Blaaderen[1], Marijn A. van Huis[1]

[1]*Debye Institute for Nanomaterials Science and Center for Extreme Matter and Emergent Phenomena, Utrecht University. Princetonplein 5, 3584 CC Utrecht, The Netherlands. [2]University of Vienna, Faculty of Physics and Center for Computational Materials Science, Sensengasse 8/12, A-1090 Vienna, Austria.*

Knowledge about the intrinsic electronic properties of water is imperative for understanding the behaviour of aqueous solutions that are used throughout biology, chemistry, physics, and industry. Calculation of the electronic band gap of liquids is challenging, because the most accurate ab initio approaches can be applied only to small numbers of atoms, while large numbers of atoms are required for having configurations that are representative of a liquid. Here we show that a high-accuracy value for the electronic band -gap of water can be obtained by combining beyond-DFT methods and statistical time-averaging. Liquid water is simulated at 300 K using a plane-wave density functional theory molecular dynamics (PW-DFT-MD) simulation using a van der Waals density functional (optB88-vdW). After applying a self-consistent GW correction the band gap of liquid water at 300 K is calculated as 7.3 eV, in good agreement with recent experimental observations in the literature (6.9 eV). For simulations of phase transformations and chemical reactions in water or aqueous solutions whereby an accurate description of the electronic structure is required, we suggest to use these advanced GW corrections in combination with statistical analysis of quantum mechanical MD simulations.

I. Introduction

Because of its importance in the natural sciences, the structure and physical properties of different phases of water have been the subject of intensive investigations by scientists and engineers for over a hundred years.[1-5] A large effort has been made to understand the structural and transport properties of water. At present the structures of gaseous and solid H_2O (ice) phases are well established, based on the early work by Fowler and Bernal who proposed that (1) each H_2O molecule can be regarded as an 'element' and (2) in building the structures of ice phases, each H_2O element is in tetragonal coordination with hydrogen bonds (O---H) of about 1.9 Å.[5] The variations of O---

H ordering in the tetragonal coordination creates dozens of ice phases, which at present are still under discussion.[5-12] Obviously, there is no long-range ordering in liquid water. However, at short-range the structure of water is topologically the same as those of ice structures, but with flexible bond-lengths and angles of H_2O tetragons.[3,5,6,12-14]

To successfully perform simulations of chemical reactions in aqueous solutions, it is imperative that not only the atomic structure, but also the electronic structure is well described, whereby the electronic band gap can serve as the most important criterion. Many studies have already been performed on the electronic band gap of liquid water, but in the cases where accurate computational methods were used, these were

applied to too few water molecules to be representative of liquid water. And in the cases where large numbers of water molecules were actually considered, methods such as cluster calculations were used which are known to be less accurate in predicting electronic properties.

Here we aim for high accuracy by applying *GW* corrections to plane-wave density functional theory (PW-DFT) molecular dynamics (MD) simulations using a van der Waals density functional and a statistical analysis by time-averaging of relevant physical parameters 'measured' during the MD simulations. We will now first discuss the experimental studies whereby the electronic structures of gas, water, and ice phases were investigated.[2,15-25] Shibaguchi and co-workers investigated the electronic structure of ice by means of a combination of X-ray photoemission spectroscopy (XPS), Ultraviolet photoemission spectroscopy (UPS), and optical absorption spectroscopy, and obtained a band gap of 8.75 eV.[17] Painter and co-workers measured the reflectance of liquid water between 1050 and 3000 Å[16] and found that the imaginary index of refraction starts at around 7.1 eV. From the measured real and imaginary parts of the index of refraction and dielectric constant, the authors suggested an exciton transition at 8.3 eV, an interband transition at 9.6 eV, and an electronic band gap of 9.0 eV.[16] Other measurements of photoemission spectra provide a range of values for the band gap of water; 6.9 eV,[21,22] 7.0,[23] 8.7 eV,[24] 8.9 eV[25] and 9.0 eV.[16] As reviewed by Winter and co-workers, such a variance in experimental data for the insulating ice phases and water is caused by many factors, such as electric charging, work functions, surface sensitivity (electron escape depths are typically ~10 to 20 Å), vapour/solid or vapour/liquid mixing, impurities, *etc*.[2,19]

Many theoretical and simulations studies have also been performed to study the structural and electronic properties of water phases. To study the structure and dynamics simple empirical potentials are widely used.[26-30] Moreover, *ab initio* Hartree-Fock (HF) and post-HF methods were employed to study water molecules and clusters, as well as ice phases[11,12,21,22,34-36]. Finally, first-principles density functional theory (DFT) has also been widely used to study the structure and electronic properties of ice phases and liquid water.[31-37]

In theoretical studies of ice and liquid water, there are several issues to be noted. First, the standard DFT functionals, such as the local density approximation (LDA) and different GGA functionals, which are local or semi-local, do not describe accurately van der Waals interactions. This is an important issue since van der Waals interactions were shown to play an important role in water and ice phases, as well as other solids.[39-50] For example, Santra and co-workers have recently investigated the ice phases at non-zero pressure using different van der Waals DFT exchange-correlation functionals and observed significant improvements of phase transition pressures of the ice phases compared to that of PBE (after the names of authors, Perdew, Burke and Ernzerhof) functional.[41,42] The van der Waals density functional was also found to describe water adsorption on metals well.[43,44,49] Second, most of the calculations performed so far have focused on the description

of the ground states of ice phases and water. However, experimental measurements of electronic properties, such as band gaps, are related to excitations of electrons. To describe the excitations another scheme needs to be used, such as the *GW* approximation (whereby the self-energy is obtained from the Green's functional *G* and the electronic screening effect *W*) which describes well the eigenstates of one-electron quasi-particle (QP) levels which relate to electronic excitations.[31,52-56] This method, but in a non-self-consistent *G0W0* fashion, was used by Hermann and co-workers to obtain the band gap of Ice-XI.[31,32] Moreover, most first-principles molecular dynamics simulations employed super-cells of 100 to 200 atoms, which can represent only a small number of molecules, and most simulations provide information about only one or a few configurations. This is not sufficient to obtain statistically meaningful results.[56,57] Consideration of a large number of configurations with sufficient molecules to probe all relevant structures is needed. This approach was applied to analyse statistically the dominant defects in hydrogenated amorphous silicon nitrides covering different stoichiometries.[57] The electronic structures were successfully simulated, including the energy gaps for the amorphous semiconductors with different types of defects.[56,57]

In the present manuscript, we report our results of a first-principles study on the H_2O molecule, its dimer and Ice-XI, a low-temperature and low-pressure H_2O phase with well-established H ordering[8,10,11,26-32] as well as molecular dynamics simulations of water at 300 K, using the van der Waals density functional developed by Dion[39] and implemented into the code VASP by Klimeš and co-workers[40]. We also employ the self-consistent *GW0* approach[52,54] for Ice-XI. The almost linear relationship that was obtained between the QP (Quasi-Particle) energies and K-S (Kohn-Sham) eigenvalues is used to obtain the electronic structure including the band gap of water. Furthermore, we also analyse the charge distributions for H_2O molecule, H_2O dimer, and charge transfer between H_2O molecules in water using the Bader charge approach[58] which has been successfully applied to many molecules[59] and crystalline solids[58,60]. Distributions of charges at O and H were obtained for the simulated water, as well as for the isolated H_2O monomer, its dimer and Ice-XI. The obtained electronic structures and the energy gaps for the ice phase and liquid water are in good agreement with available experimental data. This is not only useful for having a better understanding of the intrinsic properties of water, but also suggests that the same approach can be successfully applied to aqueous solutions that are widely used in various scientific disciplines and in industrial processes.

The paper is arranged as follows. In Section II, we introduce the (super)cells which were employed for structural optimization of an isolated H_2O molecule and its dimer, as well as of water with the experimental density at room temperature. The details of the computational methods are also described. The optimized structures of the isolated H_2O molecule, its dimer and the lattice parameters of Ice-XI are presented in Section III.A. The structural and chemical bonding details and

This journal is © The Royal Society of Chemistry 2012

Phys. Chem. Chem. Phys., 2012, **00**, 1-3 | **2**

electronic properties of first-principles molecular dynamics simulated water are presented in Section III.B. The electronic properties of Ice-XI obtained using the DFT van der Waals density functional are discussed together with the *GW0* corrections in Section III.C. In Section III.D, we discuss the electronic structure of water with the *GW* corrections. The corrected curves of the density of states (DOS) are compared with the experimental measurements (mainly photoemission spectra). Finally a brief summary is presented in Section IV.

II. Details of computational techniques

For all the structural optimizations and total energy calculations of the isolated molecules and molecular dynamics simulations, we employed the Vienna code VASP (Vienna *Ab initio* Simulation Package)[57,58] which is based on the density functional theory (DFT) within the Projector-Augmented Wave (PAW) method.[59,60] The Dion's van der Waals density functional which includes nonlocal contributions was employed for the correlation energy term.[39,40,44] The generalized gradient approximation[61] (GGA) within the optB88 functional was employed for the exchange term. The electronic wave functions were sampled on dense grids ($20 \times 10 \times 10$ or 396 irreducible *k*-points) in the Brillouin zone (BZ) of the crystals, using the Monkhorst and Pack method[62] for the total energy and electronic structure calculations of liquids and solids. Structural optimizations were performed with relaxation of both lattice parameters and coordinates of atoms for the crystals, while only atomic coordinates in a fixed cube were relaxed for the molecules.

It is noteworthy that the water and ice phase contain strong local bonds, O 2p - H 1s and therefore, the calculated valence electron total energy is expected to depend on the cut-off energies. We make a systematic investigation on the total energy calculations using different cut-off energies for the wave functions (E_{cut}) and for the augmentation functions (E_{aug}) which is about 30 % higher than the corresponding E_{cut} for a H_2O molecule. The calculated results (see Figure 1) show strong variations in the low energy range (E_{cut}/E_{aug} = 100/200 to 250/400 eV) for the calculated bond-length, the H-O-H angle and the total valence electron energy. When E_{cut}/E_{aug} is at least 300/450 eV, there is little dependence of the O-H bond-length (within 0.001 nm) and the H-O-H angle (within 0.1°) on the energy set, but still a weak dependence of the calculated total energy on the energy set. The calculated total valence electron energy becomes stable when the cut-off energy is over 650 eV (within 1 meV/atom). Therefore, to ensure cut-off independent results in all total energy calculations the cut-off energy of the wave functions was set to be 750 eV, and the cut-off energy of the augmentation functions was set to be 1000 eV. The low sensitivity of the H-O-H angle and the O-H bond-length on the cut-off energy also allows us using lower cut-off energies for the molecular-dynamics simulations. We used a cut-off energy of 320 eV, and only the Γ point in the Brillouin zone (BZ) in all molecular-dynamics simulations for the sake of finding a

reasonable balance between computational feasibility and accuracy of the results since the cell is large.
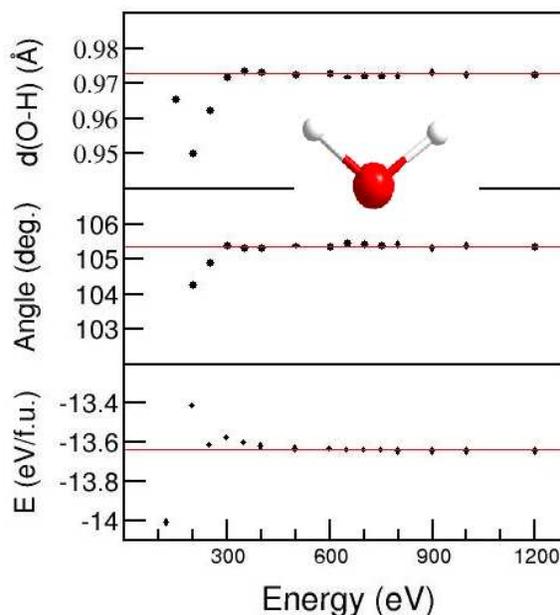

Figure 1. Convergence of the O-H bond-length (top), the H-O-H angle (middle) and the calculated total energy (bottom) as a function of the cut-off energy for an isolated H_2O molecule (schematic structure being inset) using the van der Waals density functional. The red solid lines indicate the converged values.

III. Calculated results and discussion

III.A. Structures of the H_2O molecule, H_2O dimer, and the Ice-XI phase

We first discuss the properties of a water monomer, dimer, and Ice-XI. Tables 1-4 list the calculated results for an isolated H_2O molecule and its dimer (Figure 2b), as well as the Ice-XI phase with ordered hydrogen arrangements[11,12,26] (see Figure 2a). The calculated results are compared with recent theoretical studies.[11,33, 34, 38, 47,67]

The O-H bond-length in the H_2O monomer is 0.973 Å, close to the experimental values within 0.02 Å.[64] There are many theoretical studies using various functionals, including the 'hybrid' B3LYP method which adopted an all-electron 6311G(p,d) basis set [11,12], the X3LYP which contains van der Waals interactions,[35,35] and the ab initio Hartree-Fock method within Coupled-Cluster singles, doubles, Triples (HF-CCSDT) wave function[38]. Here we compare our results with a few of them (Table 1). The obtained O-H bond is close to those obtained by the *ab initio* HF methods and by first-principles DFT approximations (Table 1). The presently calculated H-O-H angle is just about 1.0° larger than the measured one, and in good agreement with former theoretical calculations, as shown in Table 1.

This journal is © The Royal Society of Chemistry 2012

Phys. Chem. Chem. Phys.., 2012, **00**, 1-3 | **3**

Table 1. Calculated results for an isolated H_2O molecule using the optB88-vdW functional with comparison with the former theoretical works and experimental observations.

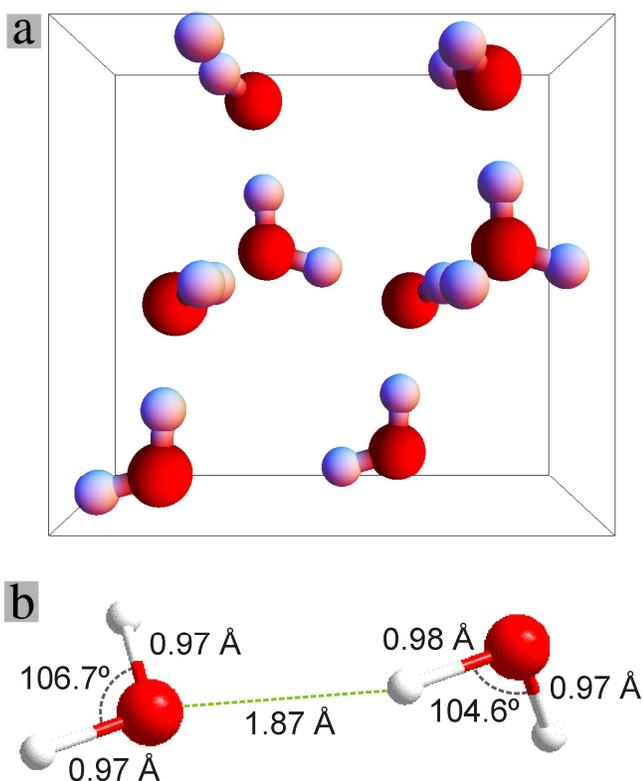|	Methods	d(O-H)(Å)	Angle H-O-H (°)
This work	optB88-vdW	0.973	105.40
Xu and Goddard [35,36]	HF	0.941	106.2
	PBEPBE	0.971	104.0
	X3LYP	0.961	105.1
Casassa,et al.[11,12]	HF-CRY-c	0.940	106.2
	B3LYP-CRY-c	0.961	105.1
	PW91-CRY-c	0.968	104.3
Silvestralli +Parrinello [34]	GGA-BLYP	0.972	104.4
Jurečka[38]	HF-CCSDT	0.959	104.2
Exp.[15]		0.957	104.5
Exp.[16]		0.958	104.45

Figure 2. (a) Schematic structure for ice Ice-XI with the projection along the [001] direction. (b) Structure of a H_2O dimer, the unit for the angles is degree, for the O-H and O---H bonds (bond lengths in Å).

Table 2 and Figure 2b also show the calculated results for the H_2O dimer. The calculated bonds and angles are in line with the former calculations. The calculated O-H bond for the H participating in the hydrogen bond (0.98 Å) is slightly longer than the other 3 short O-H bonds (0.97 Å). This difference (0.01 Å) was also obtained by other DFT and HF calculations.[11,33,34,38] The calculated binding energy is close to the experimental value, with slight overestimation, as observed previously.[12,27]

Table 2. Calculated results for an H_2O dimer using the optB88-vdW functional with comparison with the former theoretical works and experimental observations.

	Methods	d(O-H)(Å) range	d(O-O)(Å)	E_{form} (eV/f.u.)
This work	optB88-vdW	0.97/0.98	2.866	-0.236
Xu and Goddard[35,36]	HF	0.941/ 0.945	3.048	-0.16
	PBEPBE	0.970/0.981	2.899	-0.28
	X3LYP	0.957/0.968	2.908	-0.24
Casassa, et al.[11,12]	HF-CRY-c	0.944*	3.042	-0.12
	B3LYP-CRY-c	0.969	2.925	-0.21
	PW91-CRY-c	0.979	2.880	-0.24
Jurečka[38]	HF-CCSDT			-0.218
Exp.[12,17]			2.976	-0.24

*The O-H distance with hydrogen bonding with another O.

The ground state of H_2O is the Ice-XI phase.[9-12,26-30,47,69] The crystal structure of Ice-XI is orthorhombic with space group $Cmc2_1$ (nr. 36). The structure at 5 K was determined by Leadbetter and co-workers using neutron diffraction (Table 3)[69] and investigated theoretically by several groups with different approaches.[11,26,27,32,41,42]

Table 3. Calculated results for the Ice-XI phase.

Method	lattice pars. (Å), V (Å³/f.u.)	Atomic coordinates
optB88-vdW (this work)	a= 4.343(-3.5%) b = 7.609(-2.5%) c= 7.035 (-4.0%) V = 29.06 (-9.6%)	O1 4a(0,0.6502,0.0586) O2 4a(0,0.3190,0.9358) H1 4a(0,0.6571,0.2017) H2 4a(0,0.5226,0.0197) H3 8b(0.6870,0.7526,0.9811)
HF-CRY [11]	a= 4.57 (+1.5%) b = 8.40 (+7.7%) c= 7.69 (+4.9) V = 36.85(14.6%)	
B3LYP[11]	a= 4.42(-1.8%) b = 7.85(0.7%) c= 7.23 (-1.3) V = 31.36(-2.5%)	
Neutron diffraction [65]	a= 4.5019 b = 7.7978 c= 7.3280 V =32.16	O1 4a(0,0.6648,0.0631) O2 4a(0,0.3255,0.9360) H1 4a(0,0.6636,0.1963) H2 4a(0,0.5363,0.0183) H3 8b(0.6766,0.7748,0.9817)

This journal is © The Royal Society of Chemistry 2012

Phys. Chem. Chem. Phys., 2012, **00**, 1-3 | **4**

We performed full structural optimization of this ice phase using the van der Waals density functional optB88-vdW. The results are shown in Table 3. It is clear that our calculated lattice parameters are 2.5 % to 4.0 % smaller than the corresponding experimental values. That difference is similar to the PW91 results obtained by Casassa and co-workers.[11,12] We also note that HF calculations overestimate the volume while better agreement with experiment can be obtained with much more computationally expensive correlated methods, such as the Random Phase Approximation.[47]

Bader charge analysis[58] shows that there is charge transfer of 0.64 electrons per hydrogen atom from H to O. In the H_2O dimer, the charges are almost the same for the two O ions (-1.18 electrons), which is about 0.10 electrons less than that of an isolated molecule, in agreement with former calculations.[58] There are also some differences between the charges on the H atoms: the H of the long O—H bond has a charge of +0.55 electrons, which is smaller than the charges (about 0.60 electrons) on the other three H atoms. For the ice phase, the charge on the two oxygen ions is about -1.30 electrons and the H ions are charged in the range of 0.64 to 0.67 electrons, as shown in Table 4.

Table 4. The Bader charge distributions (in units of e) on the O, H atoms in the isolated H_2O monomer, a dimer, and Ice-XI.

Structure	O	H
Monomer	-1.28	0.64
Dimer	-1.18 to -1.19	0.55 to 0.61
Ice_XI	-1.30, -1.31	0.64 to 0.67

III.B. Charges in water at 300 K.

The thermal history of water simulated at 300 K is shown in Figure 3 which also includes the variation of the cohesive energy for the water system on time at 300 K. It is clearly shown that the energy lowers down with time and reaches the equilibrium after about 3.5 ps (or 7,000 iterations).

First we briefly discuss the structure of the simulated water. We monitored the processes of the molecular dynamics simulations. We observed no sign of charged ions/clusters, neither a single proton (H^+) or $(H_3O)^+$, $(H_5O_2)^+$, nor $(OH)^-$ or $(H_3O_2)^-$ or $(H_3O_2)^-$ clusters. This is understandable considering the high formation energies of such ions or charged clusters.[2,6,22] In addition, the Born-Oppenheimer approximation was used in our molecular dynamics simulations, so that proton tunnelling is neglected. However, we observed a $2(H_2O)$ cluster with a very short intermolecular (O—H) bond of 1.4 Å (Figure S1), which exists for about 50 fs. Figure 4a shows a typical configuration of water obtained from the first-principles molecular dynamics

simulations at 300 K. We analysed several configurations obtained for each of about 0.5 ps time-gap. The O-H bonds distributions in H_2O molecules together with the Bader charge distributions are shown in supplementary Figure S2. Apparently there is a strong similarity among the distributions of the intra-molecule bonds for the different configurations (snapshots at different time) with significant deviations from a regular Gaussian-type distribution. That is also true for the Bader charge distributions (Figure S2).
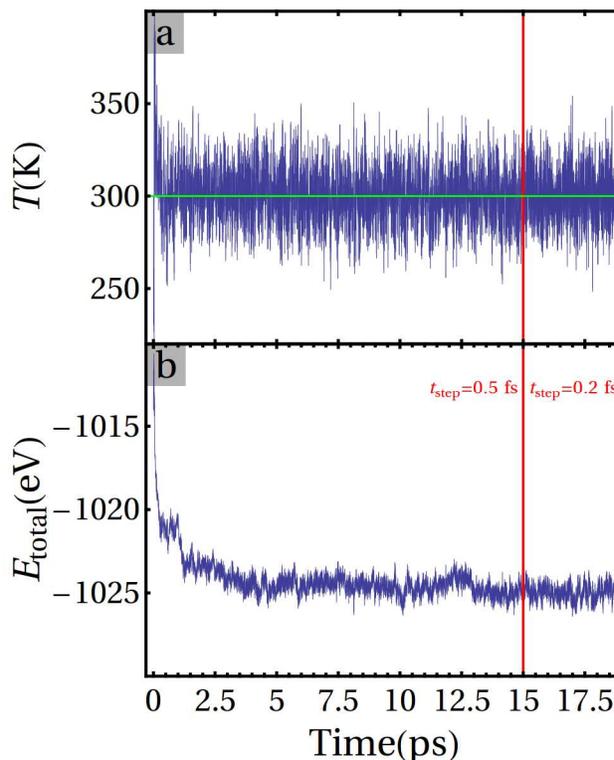

Figure 3. The thermal history of temperature (a) and total valence electron energy (b) of water simulated at a temperature of 300 K.

As discussed previously, compared with the size of a drop of water (~μm) the small number of water molecules in the cell (64 H_2O molecules, 192 atoms, size ~nm) can on the one hand be regarded as being local. The fluctuations of bonding in time, on the other hand, reflect the stochastic nature of liquid water. Therefore, time-averaging can and should be used to determine the physical properties of water. Here we simulate these properties by time-averaging over 2 ps.
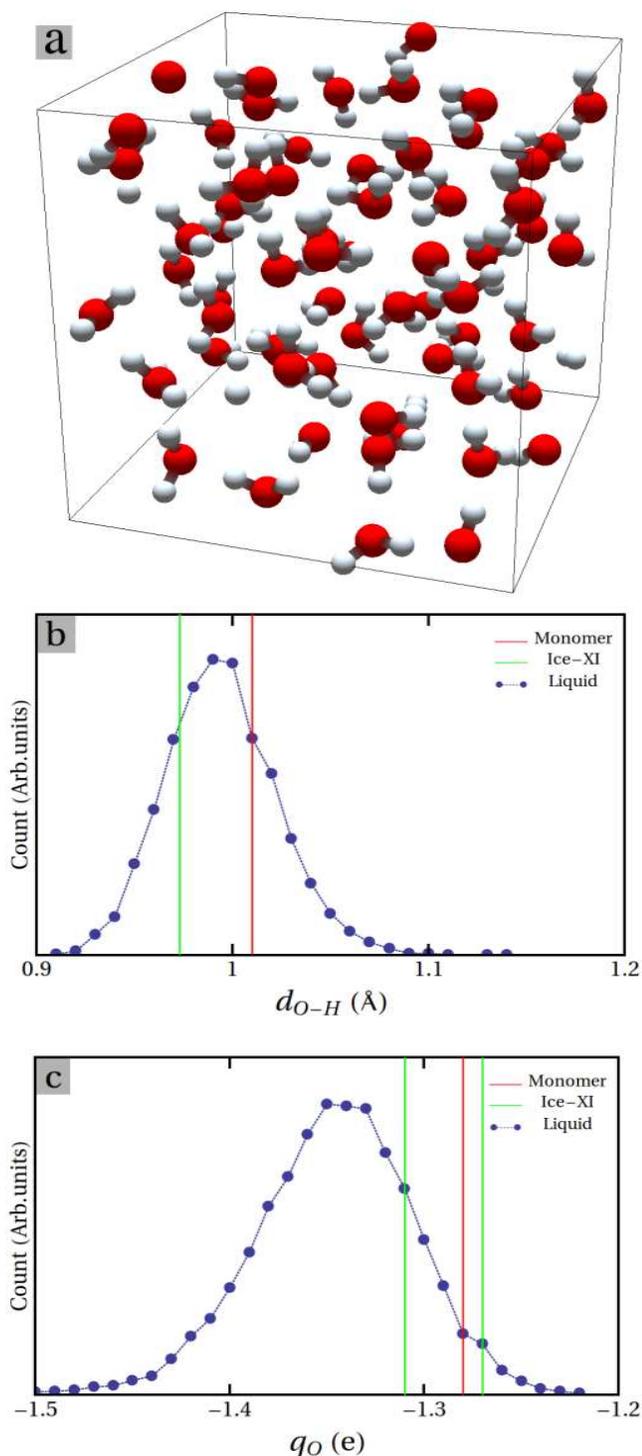
This journal is © The Royal Society of Chemistry 2012

Phys. Chem. Chem. Phys., 2012, **00**, 1-3 | 5

Figure 4. Snapshot of one typical water structure during the simulations at 300 K (a), the distributions of O-H bond lengths (b) and Bader charge of O ions (c) time-averaged over a period of 2 ps during the simulation of water at 300 K (about 100 samples).

The results are shown in Figures 4 and S2. It is clear that the time-averaged distributions show more or less regular

Gaussian-type distributions, in comparison to the large scattering observed between individual snapshot configurations (Figure S2). The O-H bond-lengths in water range from 0.92 to 1.08 Å with the width of half-peak height of 0.1 Å, centred at 0.99 Å, which is between that of isolated H_2O monomer (0.97 Å) and that in the Ice-XI phase (1.01 Å). This corresponds to the model of Bernal and co-workers.[3-5] As shown in Figure 4c, the Bader's charge at O sites of water is between -1.22 e (electrons) to -1.48 e with a broad peak at about -1.34 e. The averaged value (about 1.34 e) of the charges at O ions is slightly larger than those of an isolated H_2O monomer and Ice-XI, although the averaged O-H bond-lengths of water are close to those of the monomer and ice. This can be understood from Brown bond theory[66,67] where the valence (V_i) of the central atom to the ith neighbour is defined as

$$V_i = \exp[-(R_i - R_0)/A]$$

where R_i is the observed bond length, R_0 is a tabulated parameter expressing the (ideal) bond length when the element i has exactly valence 1, and A is an universal empirical constant, typically 0.37 Å. For example, a bond of 0.1 Å shorter gives a V value of 1.31 Valence Unit (VU) while a bond of 0.1 Å longer gives a V value of 0.76 VU. Considering the strong similarity between charge transfer and valence of atoms/ions, the higher values of charge transfer in water is understandable.

III.C. Electronic structure of Ice-XI (at 0 K) and water at 300 K

To have an overview of the electronic properties of different phases of water, the eigenvalues of an isolated H_2O molecule (5a), its dimer (5b), the total density of states for Ice-XI (5c), and one snapshot of liquid water (5d) are displayed in Figure 5. Figure 6 shows the calculated partial and total density of states (pDOS and tDOS) (6a) and the corresponding dispersion curves along the high symmetry lines of the Brillouin Zone (BZ) for the orthorhombic Ice-XI phase using the Dion's DFT-v/d Waals density functional.[39,40] The eigenvalues of the isolated H_2O molecule originate from the interactions between O 2s, O 2p, and H 1s states.[15-19,33,73] There are early assignments for the four occupied eigenstates, $2a_1$ (O 2s with some H 1s character), $1b_2$ and $3a_1$ (O 2p hybridized with H 1s), $1b_1$ (non-bonding O 2p), and the lowest unoccupied $4a_1$ (O 2s 2p and H 1s) and $2b_2$ (O2p and H 1s) states. The $2a_1$, $1b_2$ and $3a_1$ belong to bonding states while $4a_1$ and $2b_2$ have anti-bonding characters.

For the H_2O dimer, the distortion of the molecules and the interactions between the molecules (Figure 2) cause splitting (about 1.5 eV) for the $1b_2$ states, and further hybridizations between $3a_1$ and $1b_1$ states that induce the lowering of new $3a_1$ and shifting up of new $1b_1$, together with creation of two new hybridized states (bonding $3a_1/1b_1$ and anti-bonding $(3a_1/1b_1)^*$ states). The lowest unoccupied states $4a_1$ are also lowered in energy due to further hybridization. Clearly the energy gap between the occupied and unoccupied states is strongly reduced in comparison to that of the H_2O molecule.
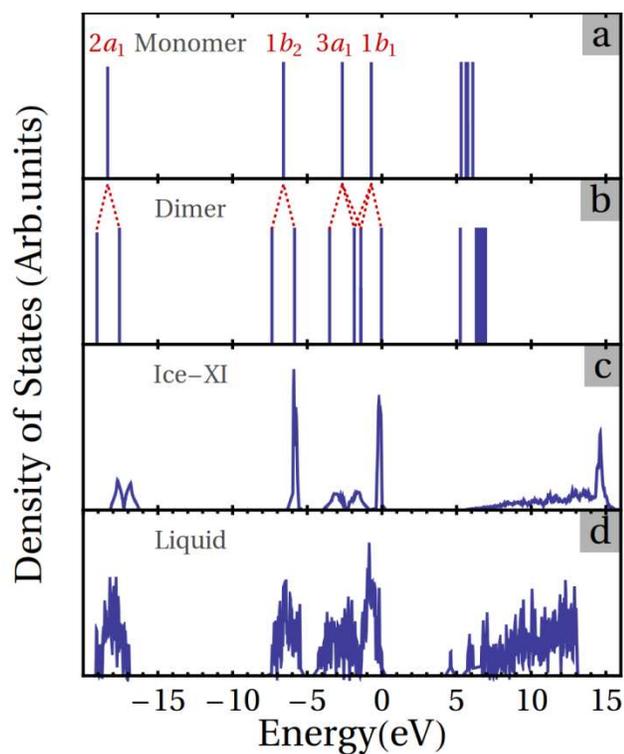
This journal is © The Royal Society of Chemistry 2012

Phys. Chem. Chem. Phys., 2012, **00**, 1-3 | **6**

Figure 5. The DFT-van der Waals density functional calculations of eigen-energies of an isolated H_2O, and its dimer; the tDOS of the ice phase and a snapshot of water simulated at 300 K with notable localization of electronic states.

Figure 5 also includes the tDOS for Ice-XI for the sake of comparison. Overall the results for the Ice-XI phase agree well with the early symmetry study by Parravicini and Resca who used the Bloch sums formed with H_2O molecule orbitals as an expansion set for cubic ice,[72] and the recent DFT-GGA calculations by Prendergast and co-workers for the Ice-Ih phase,[34] considering the strong similarities between the different H_2O ordering of these phases.[3-6,10-12] Here we briefly discuss the electronic structure of Ice-XI, with the partial DOS and dispersion curves along the high symmetry lines in Figure 6. There are five separated bands. We use here the labels used in the early assignments[15,16,73] to designate the bands. Two of them, band $1b_2$ at -6 eV, and band $1b_1$ at the top of the valence band (set to 0 eV), show an atomic-orbital behavior with very small band widths. The lowest one ($2a_1$) belongs to the O 2s states hybridized with H 1s orbitals with two peaks at about -17.7 eV and -16.8 eV, respectively. The width of the O 2s bands is about 2 eV, with the Fermi level being set at the top of the valence band. That indicates strong interactions between the O 2s and H 1s states. However, they do not contribute to the chemical bonding since both bonding and antibonding states are fully occupied.
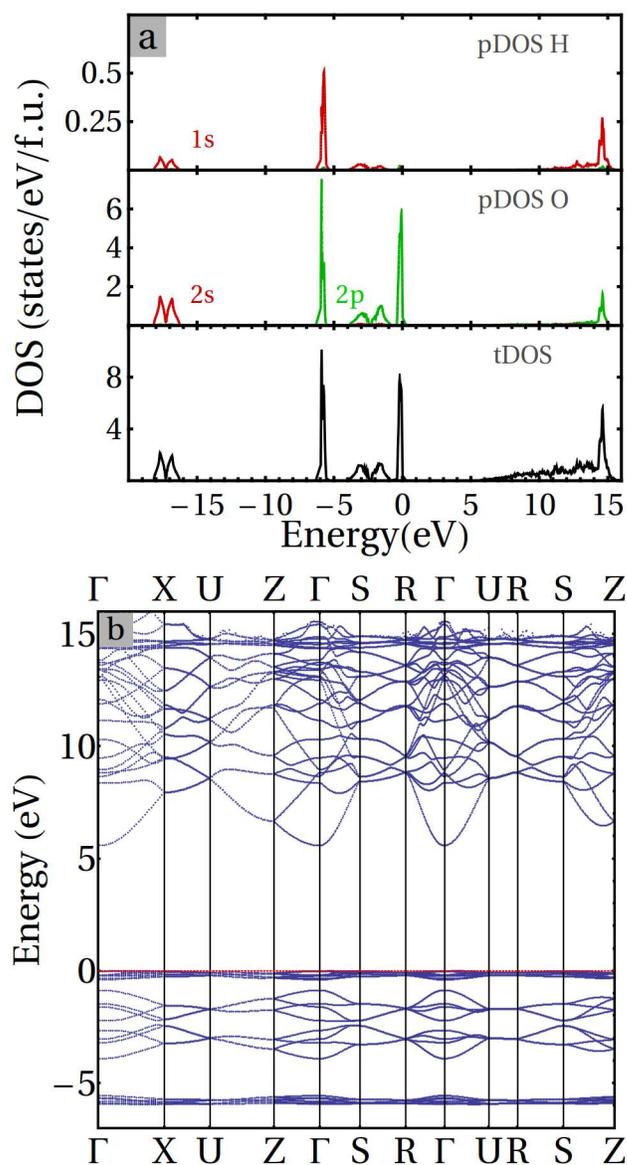

Figure 6. (a) Partial densities of states (pDOS), (b) dispersion curves along the high symmetry lines in the Brillouin zone (BZ) for the ground state of the orthorhombic Ice-XI phase. The Fermi level is set to be the top of the valence band.

There is a gap of about 10.4 eV between the O 2s band ($2a_1$) and the O 2p ($1b_2$) states with a significant hybridization with H 1s states. The very narrow band indicates a strongly localized character of the O 2p – H 1s bonding corresponding to direct bonding. The next band with two peaks at about -3.2 eV (bonding $3a_1$) and -1.6 eV (anti-bonding $3a_1^*$) is dominated by O 2p states mixed with some H 1s character. The top valence band belongs to the non-bonding O 2p states ($1b_1$). This band is very narrow and shows a strong localized character in nature.

This journal is © The Royal Society of Chemistry 2012

Phys. Chem. Chem. Phys.., 2012, **00**, 1-3 | **7**

The lower part of the conduction band (from about 5.6 to about +14.5 eV) is dominated by O 2p/3s states mixed with some H 1s character. These states in the lower conduction band show significant dispersion over 5 eV. There is a peak at about 14.5 eV dominated by O 2p – H 1s states (anti-bonding, $4a_1$).

The van der Waals density functional produced an energy gap of 5.55 eV. The top of the valence band is at (1/4,0,0) in the Brillouin Zone while the bottom of conduction band is at Γ(0,0,0). The direct energy gap at Γ is 5.58 eV, just slightly larger than that of the indirect gap. The calculated energy gap is smaller than the experimental value of 8.75 eV[17], which is not surprising since DFT functionals are known to underestimate the energy gaps of insulators and semiconductors.[52,72]

We return to Figure 5 for the electronic structure of a snapshot of water at 300 K. Though similar to that of the Ice-XI phase, the tDOS curves of water at 300 K are more dispersed: there are localized states with tailed states near the band gap. As mentioned before, the present cell containing 64 H_2O molecules can be regarded as a representative of a small fraction of a real system. Therefore, to have a better understanding about an amorphous or liquid system simulated with a limited number of atoms, statistics are required based on the number of samples, rather than based on one or a few samples, to produce physically meaningful results.[32,54,72] Water is an insulator with

strong local distortions, though topologically similar to that of ice phases.[1-3] Correspondingly the DOS curve is composed of very localized states (Figure 5). As shown in Figure 4b there are broad O-H bonds and the distributions of charges at O (Figure 4c) and at H (Figure S2) in water. It is also notable that although there is a short hydrogen bond in the 2(H_2O) clustering (Figure S1), this clustering contributes nothing to the top of valence band and bottom of conduction band, as shown in Figure S5.

That is understandable since the electronic structure of water is determined mainly by the short O-H bonds in the water molecule. In fact our analysis showed a change of Fermi level in a range of about 0.9 eV for water in 2 ps (Figure S3). Meanwhile, as shown in Figure S3, the lowest unoccupied eigen-energies vary, albeit only slightly (0.1 eV). The major change of the DOS comes from the top of valence states due to the wide local bonding. Therefore, the integrated tDOS can be considered as representative of the electronic properties of water as a whole (Figure 5). Clearly the integrated tDOS have broader bandwidths for each band. There are tailed states at the edges of valence band and conduction bands. This results in a band gap of about 3.9 eV for the present calculations, largely due to the tailed states at the top of the valence band. The overall electronic characteristics are shown in Table 5.

Table 5. Calculated electronic band gap and binding energies relative to the top of valence band ($1b_1$) for an isolated molecule and its dimer, and the peak positions of the energy bands for the Ice-XI phase and water. A selection of former theoretical calculations and experimental observations are also listed for the sake of comparison.

	Author year	Method	$(3a_1/3a_1{}^*)^b$ - $1b_1$	$(1b_2/1b_2{}^*)^b$ - $1b_1$	$(2a_1$-$2a_1{}^*)^b$-$1b_1$	ΔE_{gap}
H_2O mono.	This work	optB88-vdW	1.94^a	5.88^a	17.64^a	6.02
	Couto 2005	GGA_MPW1	2.1^{33} /	6.0^{33}		12.4^{33}
	Banna 1986	Exp.	2.20^{71}	6.18^{71}	20.02^{71}	
H_2O dimer	This work	DFT_vdW	3.47/1.82/1.38	7.33/5.82	19.04/17.54	5.29
	Couto 2005	GGA_MPW1	$3.7/2.1/1.4^{33}$	$7.5/6.1^{33}$	$23.0/21.3^{33}$	11.33^{33}
	HF	$3.5/2.0/1.3^{33}$	$7.3/6.1^{33}$	$24.6/23.2^{33}$	13.97^{33}
Ice-XI	This work	DFT_vdW	(2.99/1.47)	5.60	17.06	5.55
	GW0	(3.36 /1.65)	6.29	18.20	9.17
	Banna 1986	Exp.	1.9^{71}	5.3^{71}	18.7^{71}	8.75^{71}
	Nordlund 2008	Exp.	$(2.40/1.80)^{19}$	6.04^{19}		
Liquid	This work	DFT_vdW	1.9	5.7	17.3	~3.9
	S_GW0	2.1	6.4	19.5	~7.3
	Shibaguchi 1977	Exp.	2.35^{17}	6.18^{17}	19.40^{17}	
	Banna 1986	Exp.	2.2^{71}	6.4^{71}	20.0^{71}	
	Winter 2004	Exp	2.34^{19}	6.38^{19}	19.74^{19}	
	Nordlund 2008	Exp	2.50^{20}	6.37^{20}		
	Coe 1997,2001	Exp.				$6.9^{21,22}$

a There is only one peak for each of the $2a_1$, $1a_2$ and $3a_1$ states for one H_2O molecule (Figure 5)
b The states are overlapped for liquid water.

This journal is © The Royal Society of Chemistry 2012

Phys. Chem. Chem. Phys., 2012, **00**, 1-3 | **8**

III.D. *GW0* corrections and comparison with experimental observations

It is clear from Table 5 that there are many differences between the calculated electronic properties of the ice phase and water and the experimental photoemission spectra (PES) measurements. That is due to the fact that the DFT approaches describe well the ground states of electronic properties of materials, while most experimental methods, e.g. PES, are sensitive to the excitation of electrons. The GW method, a beyond-DFT approach, is very suitable to describe the excitation processes of sp electrons (a quasi-particle (QP) approach) and has been successfully applied for many systems.[49,50,52,53,70] Hermann and co-workers performed a non-self-consistent G0W0 correction.[31,32] The requirements for computational capability limit us to the Ice-XI phase. Figure 7 shows the results of partially self-consistent GW0 corrections for Ice-XI.

The calculations show that the direct GW0 correction has already improved the K-S energy gap (DFT-PBE) significantly. About 3 iterations are required to reach convergence (Figure 7a). Figure 7b shows that there is almost linear relationship between the QP energies and the Kohn-Sham (KS) eigenvalues for the sp electrons in Ice-XI. The first itineration (G0W0) provided an energy gap of about 8.66 eV which is strongly enhanced as compared to that (5.55 eV) from the van der Waals density functional theory. This G0W0 value to also close to that (about 8.8 eV) by Hermann and co-workers.[31,32] Furthermore, the QP energy gap from the GW0 correction is about 9.2 eV, considerably larger than that of the KS energy gap, as shown in Table 5. This obtained QP band gap is close to the experimental value, 8.75 eV.[71]

Considering the topological similarity between the regular structure of the ice phase and water, it is reasonable to use the obtained linear relationships between the QP energies and KS eigenvalues of Ice-XI as a correction to the electronic structure of water. Figure 8 shows the obtained tDOS curves for simulated water in comparison with the PES spectra.[19,20,75] Table 5 lists the obtained electronic characteristics of the eigen-energies of water and the ice phase. It is clear that the obtained vdW-DFT tDOS curves have the peaks mismatch with the experimental observations.

This can be understood from the fact that standard DFT provides the electronic properties of a solid at its ground state while the PES measurements are related to excitons of electrons, as mentioned before. There is excellent agreement between valence bands of the QP tDOS and the PES observations (also in Figure 8). The peaks of the hybridized O 2s and H 1a states ($2a_1$) match well with the PES measurements (not shown in Figure 8). Naturally, the heights/intensities of the peaks are dependent on the cross-sections of the photons with the characters of electrons, but
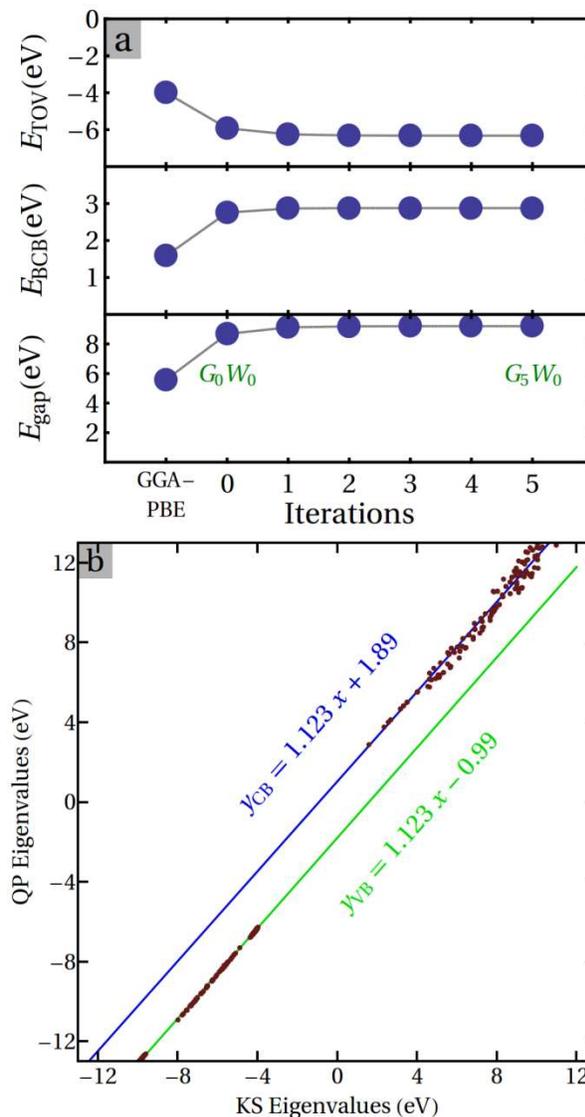

Figure 7. Convergence of the partially self-consist GW0 calculations (a), and relationships between the DFT-GGA K-S eigenvalues and GW0 QP energies (b). The green and blues lines represent the fitting functions.

the positions of the peaks can easily be recognized and are listed in Table 5. The obtained energy gap for the integrated tDOS of water at 300 K is about 7.3 eV for the QP, which is much higher than that of KS gap (about 3.9 eV). The QP gap of 7.3 eV is in between the experimental values ranging from about 6.9 to 9.0 eV. The energy gap found in the present work is slightly larger than the predicted values (6.01 to 6.55 eV) obtained from a combination of configuration interaction (CI) and time-dependent DFT (TD-DFT) calculations.[76,77] In particular, the QP gap is in

This journal is © The Royal Society of Chemistry 2012

Phys. Chem. Chem. Phys., 2012, **00**, 1-3 | **9**

very good agreement with the recent experimental measurements of the band gap of 6.9 eV.[21,22]
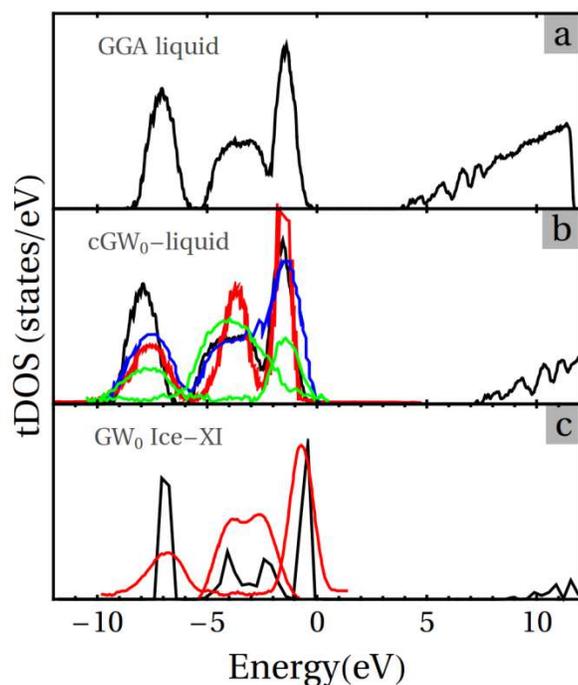

Figure 8. The time-averaged tDOS curves obtained by the optB88-vdW calculations (a) and its QP tDOS (b) of water with the *GW*-correction using the relationships between the DFT KS-eigenvalues and the *GW0* QP energies (see Figure 6 b and the corresponding text). The *GW0* tDOS curve for the Ice-XI phase is shown in the Figure (c) for sake of comparison. The Fermi level for all the curves is set to be the top of the valence bands. The colored curves in (b) and (c) are experimental measurements: in (c) the red curve for ice,[20] in (b) for water from Ref.75 (red line), from Ref. 19 (blue line) and from Ref. 20 (green lines). The black line represents the calculated results with the *GW0* corrections.

IV. Conclusions

Using the first-principles van der Waals density functional, we performed structural optimizations for the isolated H_2O monomer, its dimer, and the crystalline ice phase. The obtained results agree well with the available experimental values and former theoretical calculations. First-principles molecular-dynamics simulations for water at 300 K showed the high stability of the structural element H_2O, whereby configurations of the H_2O elements retain tetragonal coordination with distortions. Bader charge analysis showed that water is strongly ionic with a charge transfer of 0.64 e/H to O.

To describe the electronic structure and in particular the electronic band gap of liquid water with high accuracy, we

have employed the *GW* correction based on the relationship between the Kohn-Sham (KS) eigenvalues and Quasi-Particle (QP) eigenvalues of the ice phase. Moreover, we have taken about one hundred snapshot configurations of liquid water with 192 atoms in the simulation cell, and performed statistical time averaging to obtain a more reliable estimate of the physical properties. Overall, the self-consistent *GW0* corrections produce electronic structures and electronic band gaps of both Ice-XI and water that are in excellent agreement with experimental observations. The present knowledge is helpful to understand many processes and reactions in water and aqueous solutions, such as sol-gel silica processes.[78] We suggest this approach as an accurate method to investigate the electronic properties of aqueous solutions and chemical reactions therein.

Supporting Information Available: Additional Figures are available in the supporting information. This material is available free of charge via the Internet at http://pubs.RSC.uk.

*Corresponding author: C.Fang@uu.nl

References

[1] Bartels-Rausch, V.; Bergeron, J. H. E.; Cartwright, R.; Escribano, J. L.; Finney, H.; Grothe, P. J.; Gutijěrrez, J;. Haapala, W. F;. Kuhs, J. B. C.; Pettersson, S. D.; Price, C. I.; Sainz-Diaz, D. J.; Stokes, G.; Strazzulla, E. S.; Thomson, H.; Trinks; Uras-Aytemiz, N. *Rev. Mod. Phys.* **2012**, *84,* 885.

[2] Winter, B.; Fauber M. *Chem. Rev.* **2006**, *106,* 1176-1211.

[3] Bernal, J. D. *Proceed. Royal Soc. London A* **1958**, *247,* 421.

[3] Bernal, J. D. *The Proc. Phys. Sco. A.* **1949**, *62,* 537.

[5] Fowler R. H.; Bernal, J. D. *Trans. Faraday Soc.* **1933**, *29,* 1049-1056.

[6] Bernal, J. D.; Fowler R. H. *J. Chem. Phys.* **1933**, *1,* 515.

[7] Christner, B. Q.; Morris, C. E.; Foreman, C. M.; Cai, R.M.; Sands D. C. *Science* **2008**, *319* (5867), 1214.

[8] Iglev, H.; Schmeisser, M.; Simeonidis, K.; Thaller, A.; Laubereau A. *Nature* **2006**, *439* (7073), 183–186.

[9] Murray, B. J.; Knopf, D. A.; Bertram, A. K. (2005). *Nature* **2006**, *434* (7030), 202–205.

[10] Fang, Y., Xiao, B., Tao, J. M., Sun, J. W. and Perdew, J. P., Phys. Rev. B **2012**, 87, 214101.

This journal is © The Royal Society of Chemistry 2012

Phys. Chem. Chem. Phys.., 2012, **00**, 1-3 | **10**

[11]Casassa, S.; Calatayud, M.; Doll, K.; Minot C.; Pisani, C. *Chem. Phys. Lett.* **2005,** *409,* 110.

[12]Vega, C.; Abascal, J. L. F.; Debenedetti, P. G. *Phys. Chem. Chem. Phys.* **2011,** *13,* 19660.

[13]Finney, J. L. *J. Phys.: Conference Series* **2007,** *57,* 40-52.

[14]Errington, J. R.; Debenedetti, P. G. *Nature* **2001,** *409,* 318−321.

[15]Verrall, R. E.; Senior, W. A. *J. Chem. Phys.* **1968,** *50,* 2746

[16]Painter, L. R.; Hamm, R. N.; Arakawa, E. T.; Birkhoff, R. D. *Phys. Rev. Lett.* **1968,** *21,* 282-284.

[17]Shibaguchi, T.; Onuki H.; Onanka, R. *J. Phys. Soc. Jpn.* **1977,** *42,* 152-158.

[18]Timneanu, N.; Caleman, C.; Hajdu, J.; van der Spoel, D. *Chem. Phys.* **2004,** *299,* 277.

[19]Winter, B.; Weber, R.; Widdra, W.; Dittmar, M.; Fauber, M.; Hertel, I. V. *J. Phys. Chem. A* **2004,** *108,* 2625.

[20]Nordlund, D.; Odelius, M.; Bluhm, H.; Ogasawara, H.; Pettersson, L. G. W. *Chem. Phys. Lett.* **2008,** *460,* 86.

[21]Coe, J. V.; Earhart, A. D.; Cohen, M. C.; Hoffman, G. J.; Sarkas H. W.; Bowen, K. H. *J. Chem. Phys.* **1997,** *107,* 6023.

[22]Coe, J. V. *Int. Rev. Phys. Chem.* **2001,** *20,* 33-58.

[23]Grand, D.; Bernas, A.; Amouyal, E. *Chem. Phys,* **1979,** *44,* 73.

[24]Bernas, A.; Ferradini, C.; Jay-Gerin, J.-P. *Chem. Phys.* **1997,** *222,* 151.

[25]Goulet, T.; Bernas, A.; Ferradini C.; Jay-Gerin, J.-P. *Chem. Phys. Lett.* **1990,** *170,* 492.

[26]Barkema G. T.; de Boer, J. J. *Chem. Phys.* **1993,** *99,* 2059.

[27]Barkema G. T.; Newman, M. W. J. *Phys. Rev. E* **1998,** *57,* 1155.

[28]Itoh, H.; Kawamura, K.; Hondoh, T.; Mae, S. *J. Chem. Phys.* **1998,** *109,* 4894.

[29]Guisoni N.; Henriques, V. B. *J. Chem. Phys.* **2001,** *115,* 5238.

[30]Ramirez, R.; Neuerburg N.; Herro, C. P. *J. Chem. Phys.* **2012,** *137,* 134503.

[31]Hermann A.; Schwerdtfeger, P. *Phys. Rev. Lett.* **2011,** *106,* 187403.

[32]Hermann, A.; Ashcroft, N. W.; Hoffmann, R. *PNAS* **2012,** *109,* 745.

[33]Cabral do Couto, P.; Estácio, S. G.; Costa Cabral, B. J. *J. Chem. Phys.* **2005,** *123,* 054510.

[34]P. L. Silvestrelli and M. Parrinello, J. Chem. Phys. 111 (1999) 3572.

[35]Xu, X.; Goddard, W. A.,III. T *J. Phys. Chem.* **2004,** *121,* 4068.

[36]Xu, X.; Goddard, A.,III. *J. Phys. Chem. A* **2004,** *108,*2305.

[37]Nordlund, D.; Ogasawar, H.; Andersson, K. J.; Tatarkhanov, M.; Salmerón, M.; Petterson, L. G. M.; Nilson, A. *Phys. Chem. Chem. Phys.* **2006,** *8,* 1985-1993.

[38]Jurečka, P.; Šponer, J.; Černy, J.; Hobza, P. *Phys. Chem. Chem. Phys.* **2006,** *8,* 1985-1993.

[39]Dion, M.; Rydberg, H.; Schröder, E.; Langreth, D. C.; Lundqvist, B. I. *Phys. Rev. Lett.* **2004,** *92,* 246401.

[40]Klimeš, J.; Bowler, D. R.; Michelides, A. *J. Phys.: Cond Matt.* **2010,** *22,* 022201.

[41]Santra, B.; Klimeš, J.; Alfe, D.; Tkatchenko, A.; Slater, B.; Michaelides, A.; Car, R.; Scheffler, M. *Phys. Rev. Lett.* **2011,** *107,* 185701.

[42]Santra, B.; Klimeš, J.; Alfe, D.; Tkatchenko, A.; Slater, B.; Michaelides, A.; Car, R.; Scheffler, M. *J. Chem. Phys.* **2013,** *139,* 154702.

[43]Carrasco, J.; Klimeš, J.; Michaelides, A. *J. Chem. Phys.* **2013,** *138,* 024708.

[44]Román-Peréz, G.; Soler, J. M. *Phys. Rev. Lett.* **2009,** *103,* 096102.

[45]Graziano, G.; Klimeš, J.; Fernandez-Alonso, F.; Michaelides, A. *J. Phys. Condensed Matter* **2012,** *24,* 424216.

[46]Klimeš, J.; Michaelides, A. *J. Chem. Phys.* **2012,** *137,* 120901.

[47]Macher, M.; Klimeš, J.; Franchini, C.; Kresse, G. *J. Chem. Phys.* **2014,** *140,* to appear.

[48]Parr, R. G. *Annual Rev. Phys. Chem.* **1983,** *34,* 631.

[49] Ruiz, V.G., Liu, W., Zojer, E., Scheffler, M. and Tkatchenko, A., *Phys. Rev. Lett.* **2012**, 108, 146103.

[50]Rinke, P.; Qteish, A.; Neugebauer, J.; Feysoldt, C.; Schffler, M. *New J. Phys.* **2006,** *7,* 126.

[51]Kresse, G.; Marsman, M.; Hintzsche L. E.; Flage-Larsen, E. *Phys. Rev. B* **2012,** *85,* 045205.

[52]Hintzsche, L.E.; Fang, C. M.; Watts, T.; Marsman, M.; Jordan, G.; Lamers. M. W. P. E.; Weeber, A. W.; Kresse, G. *Phys. Rev. B* **2012,** *86,* 235204.

[53]Flage-Larsen, E.; Løvvik, O. M.; Fang C. M.; Kresse, G. *Phys. Rev. B* **2013,** *88,* 165310.

[54]Bader, R. F. W.; Nguyen, T. T.; Tal, Y.; *Rep. Prog. Phys.* **1981,** *44,* 893.

[55]Fang, C. M.; Van Huis, M. A.; Jansen, J.; Zandbergen, H. W. *Phys. Rev. B* **2011,** *84,* 094102.

[56]Fang, C. M.; Sluiter, M. H. F.; van Huis, M. A.; Zandbergen, H. W. *Phys. Rev. B* **2012,** *86,* 134114.

[57]Kresse, G.; Hafner, J.. *Phys. Rev. B* **1994,** *49,* 14251-14269.

[58]Kresse, G.; Hafner, J. *Phys. Rev. B* **1994,** *49,* 14251.

[59]Blöchl P. E. *Phys Rev B* **1994,** *50,* 17953-979.

[60]Kresse G, Furthmüller J. *Phys Rev B* **1999,** *54,* 11169.

[61]Perdew, J. P.; Burke, K.; Ernzerhof, M. *Phys. Rev. Lett.* **1996,** *77,* 3865–3868.

[62]Monkhorst, H. J.; Pack, J.D. *Phys. Rev. B.* **1976,** *13,* 5188

[63]Pereira, J. C. G.; Catlow, C. R. A.; Price, G. D.; Almeida, R. M. *J. Sol-gel Sci. Techn.* **1997,** *8,* 55.

[64]Curtiss, L. A.; Pople, J. A. *J. Mol. Spectrosc. 1975, 55,* 1.

[65]Leadbetter, A. J.; Ward, R. C.; Clark, J. W.; Tucker, P. A.; Matsuo, T.; Suga, H. *J. Chem. Phys.* **1985,** *82,* 424.

[66]Brown, I. D. *The Chemical Bond in Inorganic Chemistry. IUCr Monographs in Crystallography 12,* Oxford Science Publications, Oxford University Press, Oxford, U.K., 2002.

[67]Brown, I. D. *Chem. Rev.* **2009,** *109,* 6858-6919.

[68]Parravicini, G. P.; Resca, L. *Phys. Rev. B* **1973,** *8,* 3009.

[69]Goddard, W. A., III; Hunt, W. J. *Chem. Phys. Lett.* **1974,** *24,* 464.

[70]Hintzsche, L. E.; Fang, C. M.; Marsman, M.; Jordan, G.; Lamers, M. W. P. E.; Weeber, A. W.; Kresse, G. *Phys. Rev. B* **2013,** *88,* 155204.

[71]Banna, M. S.; McQuaide, B. H.; Malutzki, R.; Schmidt, V. *J. Chem. Phys.* **1986,** *84,* 4739.

[72]Tuckerman, M. E.; Marx, D.; Parrinello, M. *Nature* **2002,** *417,* 925.

[73]Hassanali, A.; Prakash, M. K.; Eshet, H.; Parrinello, M. *PNAS,* **2011,** *108,* 20410.

[74]Trinh, T. T.; Jansen, A. P. J.; Van Santen, R. A; Meijer, E. J. *J. Phys. Chem. C Lett.* **2009,** *113,* 2647.

[75]Chen, K. C.; Tsuchiya, T.; Mackenzie, J. D.. *J. Non-Crystal. Solids* **1986,** *81,* 227.

[76]Brancat, G.; Rega, N.; Barone V., *Phys. Rev. Lett.* **2008**, *100*, 107401.

[77]do Couto P. C.; Costa Cabral, B. J., *J. Chem. Phys.* **2007**, *126*, 014509.

[78]Xia, F. F.; Zeng, D. W.; Yi, H. B.; Fang, C. H. *J. Phys. Chem. A* **2013,** *117,* 8468.

Physical Chemistry Chemical Physics Accepted Manuscript

This journal is © The Royal Society of Chemistry 2012

Phys. Chem. Chem. Phys.., 2012, **00**, 1-3 | **12**